AEDC-TR-69-57

WIND TUNNEL TESTS ON THE APACHE SOUNDING ROCKET WITH VARIOUS SPIN RATES AT SUPERSONIC SPEEDS

James C. Uselton and Jack B. Carman
ARO, Inc.

May 1969

VON KÁRMÁN GAS DYNAMICS FACILITY
ARNOLD ENGINEERING DEVELOPMENT CENTER
AIR FORCE SYSTEMS COMMAND
ARNOLD AIR FORCE STATION, TENNESSEE

WIND TUNNEL TESTS ON THE APACHE SOUNDING ROCKET WITH VARIOUS SPIN RATES AT SUPERSONIC SPEEDS

James C. Uselton and Jack B. Carman
ARO, Inc.

FOREWORD

The work reported herein was done for and at the request of the Air Force Armament Laboratory (AFATL) and under the direction of Mr. C. B. Butler (ATBR), as a part of Program Element No. 62701F, Project No. 2547.

The results of tests presented were obtained by ARO, Inc. (a subsidiary of Sverdrup & Parcel and Associates, Inc.), contract operator of the Arnold Engineering Development Center (AEDC), Air Force Systems Command (AFSC), Arnold Air Force Station, Tennessee, under Contract F40600-69-C-0001. The tests were conducted from December 9 to December 17, 1968, under ARO Project No. VT0860. The manuscript was submitted for publication on February 12, 1969.

This technical report has been reviewed and is approved.

Eugene C. Fletcher
Lt Colonel, USAF
AF Representative, VKF
Directorate of Test

Roy R. Croy, Jr.
Colonel, USAF
Director of Test

ABSTRACT

Aerodynamic characteristics were investigated for a 0.355-scale model of the Apache sounding rocket at Mach numbers 2 to 6. Free-stream Reynolds number, based on model length, was varied between 6.5×10^6 and 23.9×10^6, and angle of attack varied from -5 to 15 deg. The model was tested without fins at spin rates up to 4,000 rpm and with fins at cant angles of 0, -1, and ±2 deg, which produced spin rates ranging from about -3200 to 3200 rpm. Tests of the complete spinning model showed significant changes in side loading with angle of attack, Mach number, and Reynolds number. Tests of the model with and without fins allowed a degree of accessment of the relative body and fin Magnus contributions. Tests of the nonspinning model with and without fins showed significant side loads attributed to steady asymmetric leeward vortex patterns.

BLANK PAGES
IN THIS
DOCUMENT
WERE NOT
FILMED

CONTENTS

APPENDIXES

I. ILLUSTRATIONS

Figure

NOMENCLATURE

A	Reference area, model base area, 4.191 in.^{2}
C_m	Pitching-moment coefficient, pitching moment/q_∞Ad
C_N	Normal-force coefficient, normal force/q_∞A
C_n	Yawing-moment coefficient, yawing moment/q_∞Ad (see Fig. 2)
C_Y	Side-force coefficient, side force/q_∞A (see Fig. 2)
d	Model base diameter, 2.310 in.
ℓ	Model length, 49.766 in.
M_∞	Free-stream Mach number
p	Model spin rate (positive, clockwise viewing from base), rpm or rad/sec
p_c	Tunnel stilling chamber pressure, psia
$pd/2V_\infty$	Helix angle or spin parameter, rad
q_∞	Free-stream dynamic pressure, psia

Re_ℓ	Free-stream Reynolds number based on model length
T_o	Tunnel stilling chamber temperature, °R
V_∞	Free-stream velocity, ft/sec
α	Angle of attack, deg
δ	Fin cant angle (positive angles produce positive spin rates), deg
ΔC_Y	$(C_Y)_{\delta=2} - (C_Y)_{\delta=-2}$
ΔC_n	$(C_n)_{\delta=2} - (C_n)_{\delta=-2}$
ϕ	Model roll angle, deg

SECTION I
INTRODUCTION

The Nike-Apache or Nike-Cajun (the Apache and Cajun are geometrically similar) is a two-stage, solid-propellant, rocket vehicle, jointly developed by NASA and University of Michigan as a meteorological sounding rocket system. These rocket systems have been successfully used in free-flight investigations to measure atmospheric densities, winds aloft, and to photograph hurricanes. These missions were successful as long as the vehicle had a reasonable static margin and flew zero lift and nonspinning trajectories. Some systems were spun up during flight either to satisfy payload requirements or for range safety reasons, and some of these flights resulted in the Apache vehicle experiencing angular motions which were unexpectedly large. For example, some vehicles went unstable and coned through large angles; others had their flights terminated abruptly because of structural failure. As a result of these flights, the roll characteristics of the Apache were investigated and are reported in Ref. 1.

Personnel at the Air Force Armament Laboratory initiated this test program to obtain the Magnus characteristics of the Apache to use in a six-degree-of-freedom stability analysis being done for them by the Notre Dame Aerospace Department.

Force data were obtained on the 0.355-scale Apache model at Mach numbers 2, 3, 4, 5, and 6 at Reynolds numbers (Re_ℓ) ranging from 6.5 million to 23.9 million. The angle-of-attack range was from -5 to 15 deg. The model was tested with and without fins, and the spin rate varied between 0 and approximately 4,000 rpm.

SECTION II
APPARATUS AND PROCEDURE

2.1 WIND TUNNEL

Tunnel A is a continuous, closed-circuit, variable density wind tunnel with an automatically driven flexible-plate-type nozzle and a 40- by 40-in. test section. The tunnel can be operated at Mach numbers from 1.5 to 6 at maximum stagnation pressures from 29 to 200 psia, respectively, and stagnation temperatures up to 750°R ($M_\infty = 6$). Minimum operating pressures range from about one-tenth to one-twentieth of the maximum at each Mach number.

2.2 MODEL

The 0.355-scale Apache model (Fig. 1, Appendix I) was designed and built at the von Kármán Gas Dynamics Facility (VKF) and is essentially an ogive-cylinder with cruciform 53-deg swept fins mounted at the model base and has a fineness ratio of 24.88. Model details are given in Fig. 2.

The model was mounted on two ball bearings with their inner races fixed to an inner shell that was attached to the balance forward taper. The model was tested with and without the fins. The model spin rates for the fins-on were obtained by canting the fins at angles of 0, -1, and ±2 deg. The model spin rates for the no-fin configuration were obtained by directing jets of nitrogen on the model base which was machined with small slanted cups for spinning. All model configurations were dynamically balanced at the VKF.

2.3 FORCE BALANCE

The VKF four-component balance shown in Fig. 3 was used for the tests. The small outrigger side beams of the balance, with semiconductor strain gages, were used to obtain the sensitivity required to accurately measure small side loads while maintaining adequate balance stiffness for the larger pitch loads. When a yawing moment is imposed on the balance, secondary bending moments are induced in the side beams. Thus, the outrigger beams act as mechanical amplifiers, and a normal-force to side-force capacity ratio of 20 was achieved for a 500-lb normal-force loading. Before the tests, a range of static loads was applied to the balance to simulate the model loads anticipated during testing. All balance components were loaded simultaneously, and a range of uncertainties in measurement was determined from the differences between the applied loadings and the values calculated by the balance calibration equations used in the final data reduction. Listed below are the ranges of static loads applied and the corresponding uncertainties for the balance components loaded singly and simultaneously:

Balance Component	Range of Static Loadings	Range of Uncertainties
Normal Force, lb	25 - 200	0.7 - 0.7
Pitching Moment, in.-lb	250 - 1000	4 - 4
Side Force, lb	1 - 6	0.015 - 0.015
Yawing Moment, in.-lb	3 - 24	0.035 - 0.10

2.4 TEST PROCEDURE AND CONDITIONS

For the zero spin data, the model was locked (ϕ = 0) by pinning the outside shell of the model to the fixed inner shell. When the model was tested with the canted fins, it was allowed to free spin at its steady-state value. Up to five data points were taken at each angle of attack when the model was spinning, whereas two or three data points were usually taken with the model locked (zero spin). The numerous data points were taken to average the scatter encountered because of model vibration and the small magnitude of the side forces.

For the no-fin spin data, the model was prespun by two nitrogen jets acting on machined cups in the model base. When the desired speed (approximately 4,000 rpm) was reached, the nitrogen supply was cut off, and data were recorded as the model spin rate decayed. Model spin rates were monitored using a photo cell-diode tachometer mounted inside the model.

The tunnel and test conditions are listed in Table I, Appendix II.

SECTION III
RESULTS AND DISCUSSION

Spinning canted fin models are normally subject to Magnus effects primarily caused by the body, blanketing of the leeside fin, and the couple created by the axial components of the normal forces on the fins. Explanations of these different types of Magnus effects are found in Refs. 2, 3, 4, and 5. Both the body Magnus force and canted fin blanketing Magnus force produce negative side forces for positive spin direction and angles of attack. The couple created by the axial components of the normal forces on the fins produces a negative yawing moment for positive spin direction and angle of attack.

In 1966, a wind tunnel program investigating the Magnus effects on the Tomahawk vehicle was conducted. The Tomahawk is a 23.3 fineness ratio sounding rocket with cruciform fins and is very similar to the Apache vehicle of this investigation. In the Tomahawk program, it was determined that, as the angle of attack was increased, the leeward wake became characterized by a steady asymmetric vortex shape that produced side forces and moments on the model for the no-spin condition. Also, it was found that the asymmetric leeward wake could cause the side force and moment curves for opposite directions of spin not to be mirror images with variation in angle of attack. In the Tomahawk tests,

the asymmetric wake effects were thoroughly investigated, and the complete results are presented in Ref. 2 along with the findings of other investigators pertaining to asymmetric wake effects. Since the Apache model of the current tests is so similar to the Tomahawk, similar trends in the data were expected.

As discussed earlier in Section 2.4, up to five data points were taken at each angle of attack to minimize extraneous points. All of the data points were plotted, and a weighted fairing was made through the data. The weighted data are presented in this report.

In Fig. 4, the variations in the side-force coefficient, C_Y, and yawing-moment coefficient, C_n, with angle of attack for the zero spin condition, fins-on at zero cant angle (δ = 0, M_∞ = 2 through 6), and fins-off (M_∞ = 3, 4, and 5) are presented for each of the Reynolds numbers tested. The data indicate the presence of the asymmetric vortex pattern mentioned earlier and discussed in detail in Ref. 2. The data indicate that the magnitude of the effect of the asymmetric vortex pattern was reduced at the higher Mach numbers and also was lower at the higher Reynolds numbers for any one Mach number. This reduction with Mach number was also noted by Cowen (Ref. 6) and by Uselton (Ref. 2).

The variations of spin rate, p, and spin parameter, $pd/2V_\infty$, with angle of attack are given in Figs. 5 and 6, respectively, for the various fin cant angles and Mach numbers. There was no notable change in the spin rate between the Reynolds numbers at any one Mach number; and, therefore, only one set of data at each Mach number is presented. Throughout the report the data obtained with the model spinning will be identified by the fin cant angle, and the reader may refer to Fig. 5 to determine the spin rate. The spin rate was near constant over the angle-of-attack range tested for most of the configurations, and no analysis of any of the small variations was attempted since no attempt was made to monitor the bearing friction or to hold it constant.

In Fig. 7, the variations of C_Y and C_n with angle of attack are presented for fin cant angles of 0, -1, -2, and 2 deg at M_∞ = 3, 4, and 5. There are several interesting points to be noted in these data. First, the data (δ = 2 and -2 deg) are very symmetric about the α axis at the lower angles of attack. At the higher angles of attack where the zero spin data are affected by the asymmetric vortex pattern, the spin data in some cases are not symmetric for the two different spin directions. This is especially apparent in the M_∞ = 3 yawing-moment data (Fig. 7a) where the data are symmetric to approximately α = 6 deg, and then the -2-deg canted fin data breaks downward in a similar manner to the +2-deg data.

A second notable characteristic of these data is the nonlinearity exhibited in the yawing-moment curve at $M_\infty = 4.01$, $Re_\ell = 10 \times 10^6$ at the low angles of attack ($\alpha = \pm 3$ deg). The sharp slope reversal is well defined and symmetrical for positive and negative angles of attack for both spin directions. This effect is also present, but not as pronounced, in the $M_\infty = 2.99$, $Re_\ell = 15.4 \times 10^6$ and $M_\infty = 5.04$, $Re_\ell = 11.9 \times 10^6$ data. Since on a free-spinning canted fin model the Magnus force or moment from the fins could cause a nonlinearity at the lower angles of attack (Refs. 2 and 3), one might suspect this to have been the cause of the slope reversal in the data. However, it will be shown later that this effect was not dependent on the fins.

Another interesting feature of the data in Fig. 7 is the sign change in the yawing moment between $M_\infty = 5$ and 3. The data show, for example, a positive C_n for $\delta = +2$ deg at $M_\infty = 5$ (Fig. 7c) and a negative C_n for $\delta = +2$ deg at $M_\infty = 3$ (Fig. 7a). This effect was possibly caused by the fin normal-force couple and/or the body Magnus force (with its more forward center-of-pressure location) becoming more dominant at the lower Mach numbers.

The spin effects can be seen more clearly in Fig. 8 where the variations of $\Delta C_Y/2$ and $\Delta C_n/2$ with angle of attack are presented for $M_\infty = 3$, 4, and 5. The local slope reversals in the yawing-moment coefficient curve at $M_\infty = 4.01$, $Re_\ell = 10 \times 10^6$, and $M_\infty = 3$, previously discussed, are easily seen. Also, the data show the sign change in the slope of the yawing-moment coefficient curve between $M_\infty = 3$ and 4. The Reynolds number effect is more pronounced at $M_\infty = 3$.

The effects of the fins on the side-force and yawing-moment variations with angle of attack for the spinning model are shown in Fig. 9. The data for the no-fin model are presented at a spin rate equivalent to that for the fins-on configuration at $\delta = -1$ and -2 deg. The data are presented for $M_\infty = 3$, 4, and 5. The fin effects are different for the three different Mach numbers. At $M_\infty = 4$, the data for the fins-on and fins-off conditions are similar and, thus, indicate that the body Magnus force is predominant. Also, since the spin rate is negative, the body Magnus force and canted fin Magnus force (from blanketing the leeside fin, Refs. 2 and 3) should be positive, which the data show.

The $M_\infty = 5$ data of Fig. 9 also show the correct direction for the Magnus force. However, the magnitude of the no-fin data is low compared to that of the fins-on data, thus indicating at $M_\infty = 5$ that the body Magnus force is low. The fin Magnus force caused by blanketing the leeside fin (Refs. 2 and 3) will first increase with angle of attack and then decrease back toward zero. The leeward fin should be enclosed

by the wake at a relatively low angle ($\alpha < 10$ deg). Since the data at $M_\infty = 5$ indicate that the classical body Magnus force was low and since the force from the leeside fin, being blanketed, should approach zero at $\alpha = 10$ deg, the fin data, because of the continued increase in magnitude with angle of attack, indicate another type of Magnus force. This continued increase in the side force and moment is believed to have been caused by the interaction of the fins with the body vortex system.

At $M_\infty = 3$ (Fig. 9), the data indicate both body and fin Magnus force and moment contributions. The substantial differences in the yawing moment, while the side force trends are similar, suggest strongly the importance of the moment created by the axial components of the fin normal forces since this effect produces only a yawing couple and no side force.

As discussed earlier and shown in Fig. 7, the $M_\infty = 4.01$, $Re_\ell = 10 \times 10^6$ data show a sharp slope reversal occurred at $\alpha = \pm 3$ deg. The suspicion that this was caused by the blanketing of the leeside fin is proved incorrect since the data of Fig. 9 show that a similar trend exists for the no-fin configuration.

The variations of C_Y and C_n with spin rate for the fins-off configuration are shown in Fig. 10 for $M_\infty = 3$, 4, and 5. Since these data are for the body alone, they indicate solely the body Magnus force and moment. The data show a decrease in the body Magnus force with increasing Mach number; and at $M_\infty = 5$, as noted earlier in Fig. 9, the body Magnus force and moment is small. The data indicate an increase in the dependence of the coefficients on rpm (p = 1500 to 4000 rpm) as the angle of attack is increased up to the higher angles. At the higher angles, the data show almost no dependence on the rpm. To understand this phenomenon, one must consider the zero spin data which show side forces and moments at the higher angles caused by the asymmetry of the leeside flow pattern. At the higher angles of attack, the leeward wake becomes asymmetric for vehicles of this type (high fineness ratio) regardless of spin rate. Therefore, at these higher angles of attack, the spin will influence the direction of the leeside wake asymmetry, but will not greatly affect the amount.

The variations of the normal-force and pitching-moment coefficients with angle of attack are presented in Fig. 11 for the fins-on configuration and in Fig. 12 for the fins-off configuration. The data are shown only for the zero canted fins to maintain clarity since it has been reported previously (Refs. 2, 7, and 8) and substantiated by the data obtained in this test that there is no discernible effect of spin on the normal force and pitching moment for the spin rates of the magnitudes of this test.

The fins-on data (Fig. 11) show the normal force and restoring moment to decrease with increasing Mach number. A theoretical calculation of C_N and C_m, using the method of Allen and Perkins (Ref. 9) for the body and an equivalent two-dimensional analysis (Ref. 10) on the fins, is included with the data. The theory is seen to be particularly good at the lower angles of attack.

REFERENCES

1. Falanga, Ralph A. "Supersonic Investigation of a Spinning and Nonspinning Model of a Cajun (or Apache) Rocket Vehicle with Roll-Control Tabs." NASA TN D-2576, January 1965.
2. Uselton, J. C. "Investigation of the Magnus Effects and the Effects of Unsymmetrical Leeward Vortex Patterns on a High Fineness Ratio Model at Mach Numbers 3 and 5." University of Tennessee, Master of Science Thesis, August 1966.
3. Platou, Anders S. "Magnus Characteristics of Finned and Nonfinned Projectiles." AIAA Journal, Vol. 3, No. 1, January 1965, pp. 83-90.
4. Platou, Anders S. "The Magnus Force on a Finned Body." BRL Report 1193, March 1963.
5. Benton, Edward R. "Supersonic Magnus Effect on a Finned Missile." AIAA Journal, Vol. 2, No. 1, January 1964, pp. 153-155.
6. Gowen, Forrest E. "Buffeting of a Vertical Tail on an Inclined Body at Supersonic Mach Numbers." NACA RM A53A09, March 1953.
7. Platou, Anders S. "The Magnus Force on a Short Body at Supersonic Speeds." BRL Report 1062 (AD 212064), January 1959.
8. DeGrafft, William E. "Wind Tunnel Investigation of the Forces and Moments Acting on a Cruciform Finned Model with Fixed and Freely Spinning Tail Assemblies at a Mach Number of 2.0." NOL-TR-63-79, April 1963.
9. Allen, H. Julian and Perkins, Edward W. "Characteristics of Flow over Inclined Bodies of Revolution." NACA RM A50L07, March 1951.
10. Shapiro, Ascher H. The Dynamics and Thermodynamics of Compressible Fluid Flow, Vol. II. Ronald Press Company, New York, 1954.

APPENDIXES

I. ILLUSTRATIONS

II. TABLE

Fig. 1 Photograph of Apache Model Installed in Tunnel A

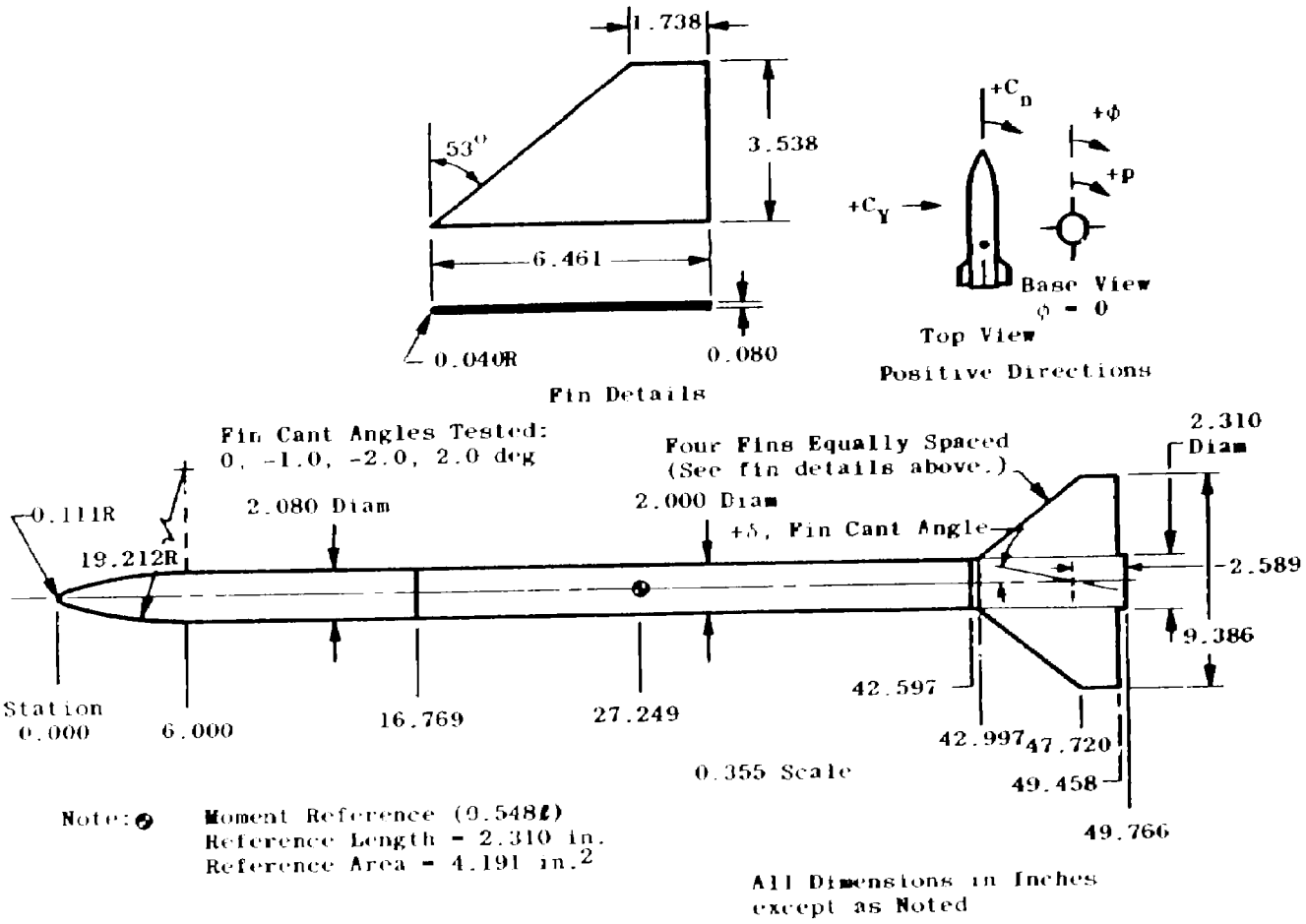

Fig. 2 Model Details

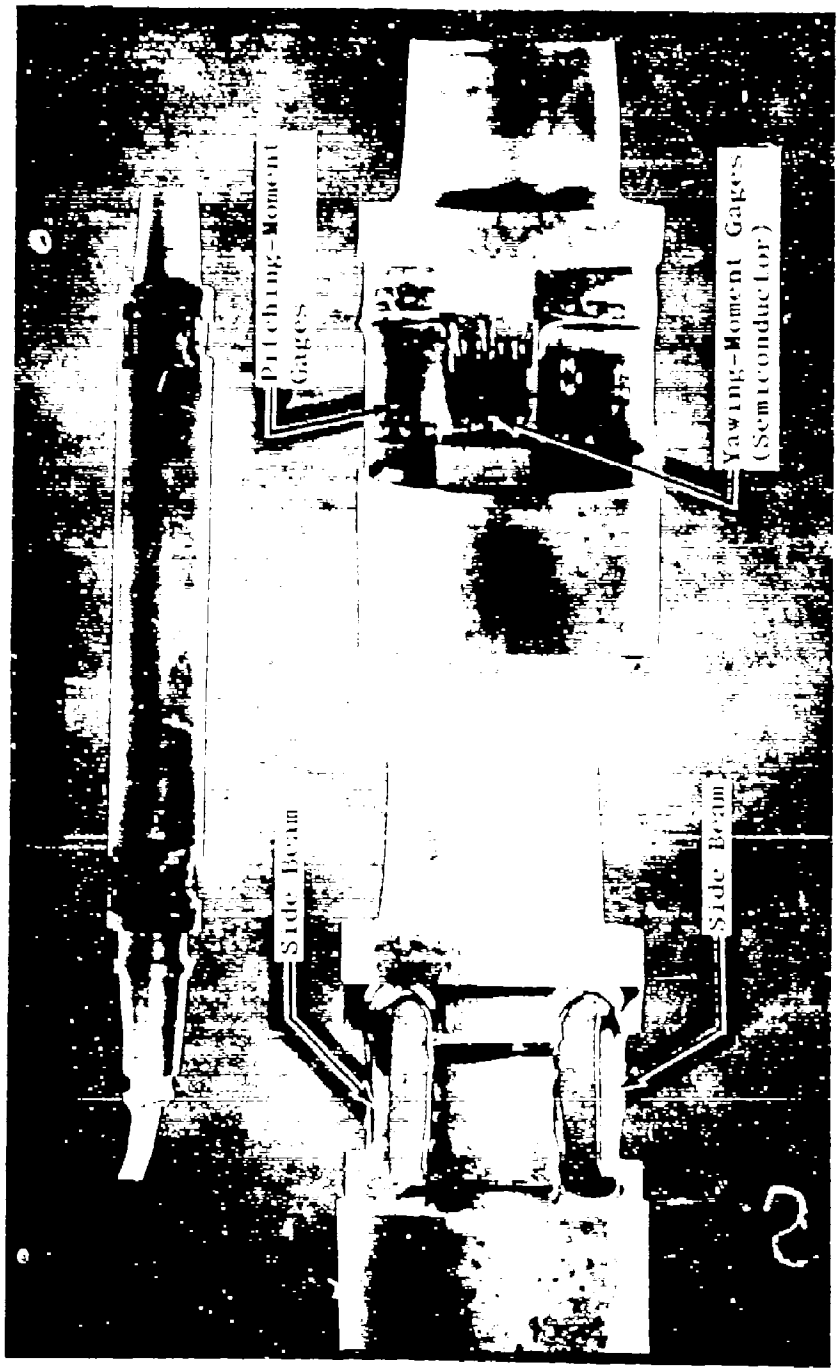

Fig. 3 Balance Details

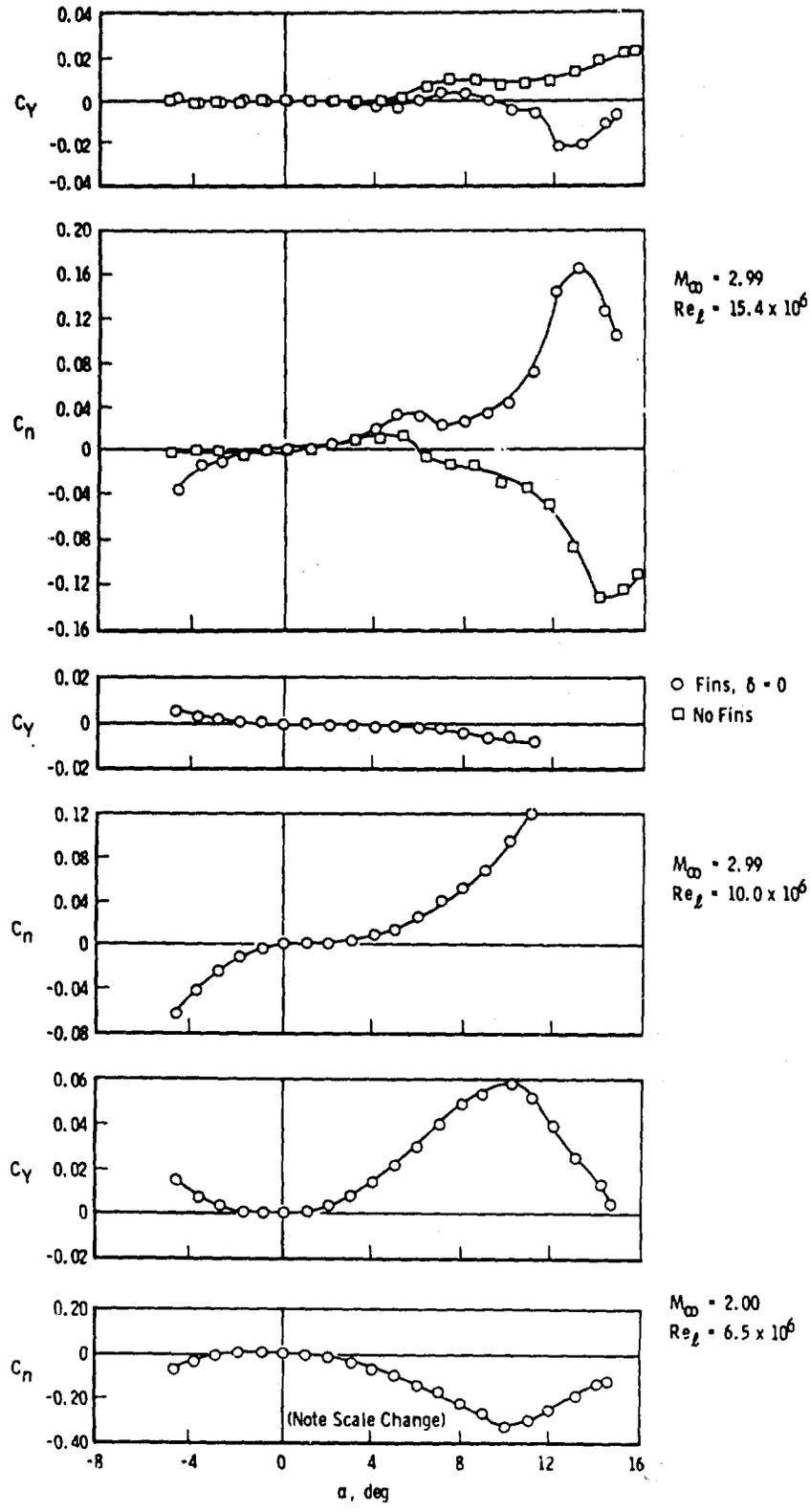

a. M_∞ = 2 and 3

Fig. 4 Variations of C_Y and C_n with α for p = 0, Fins-On (δ = 0) and Fins-Off

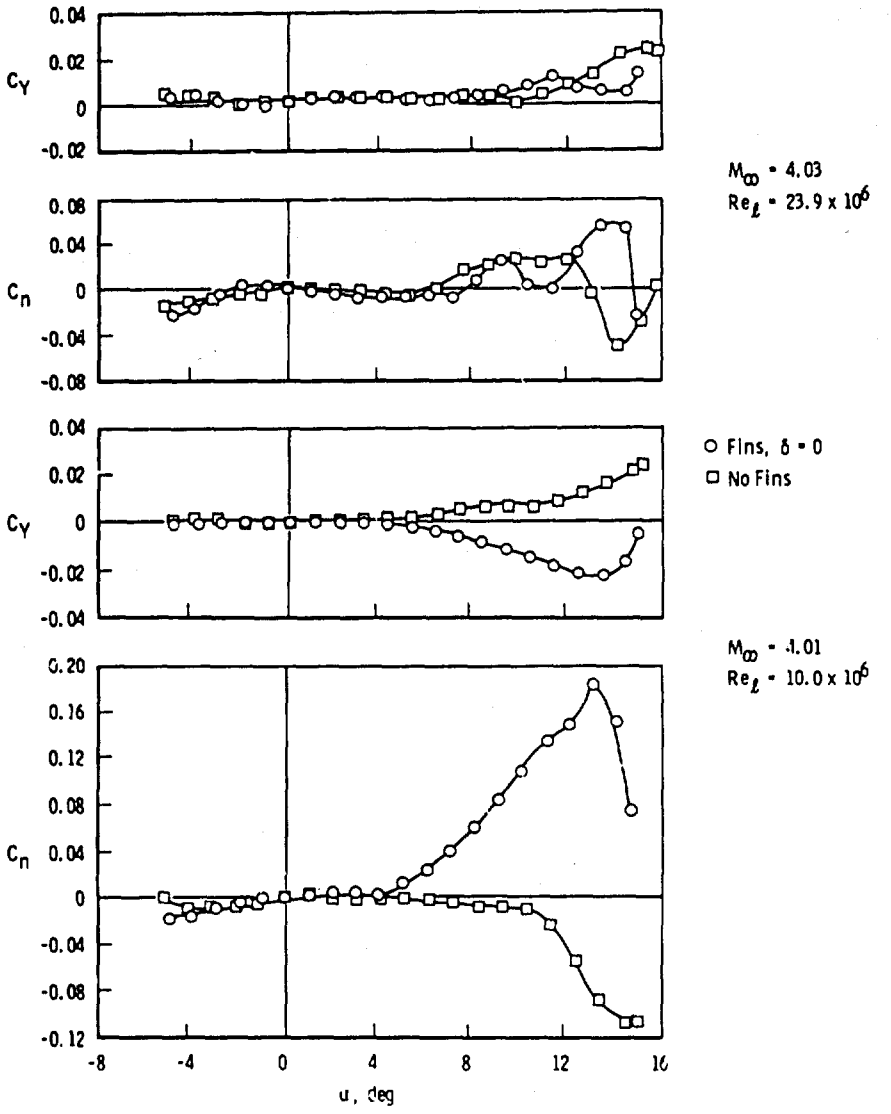

b. M_∞ = 4

Fig. 4 Continued

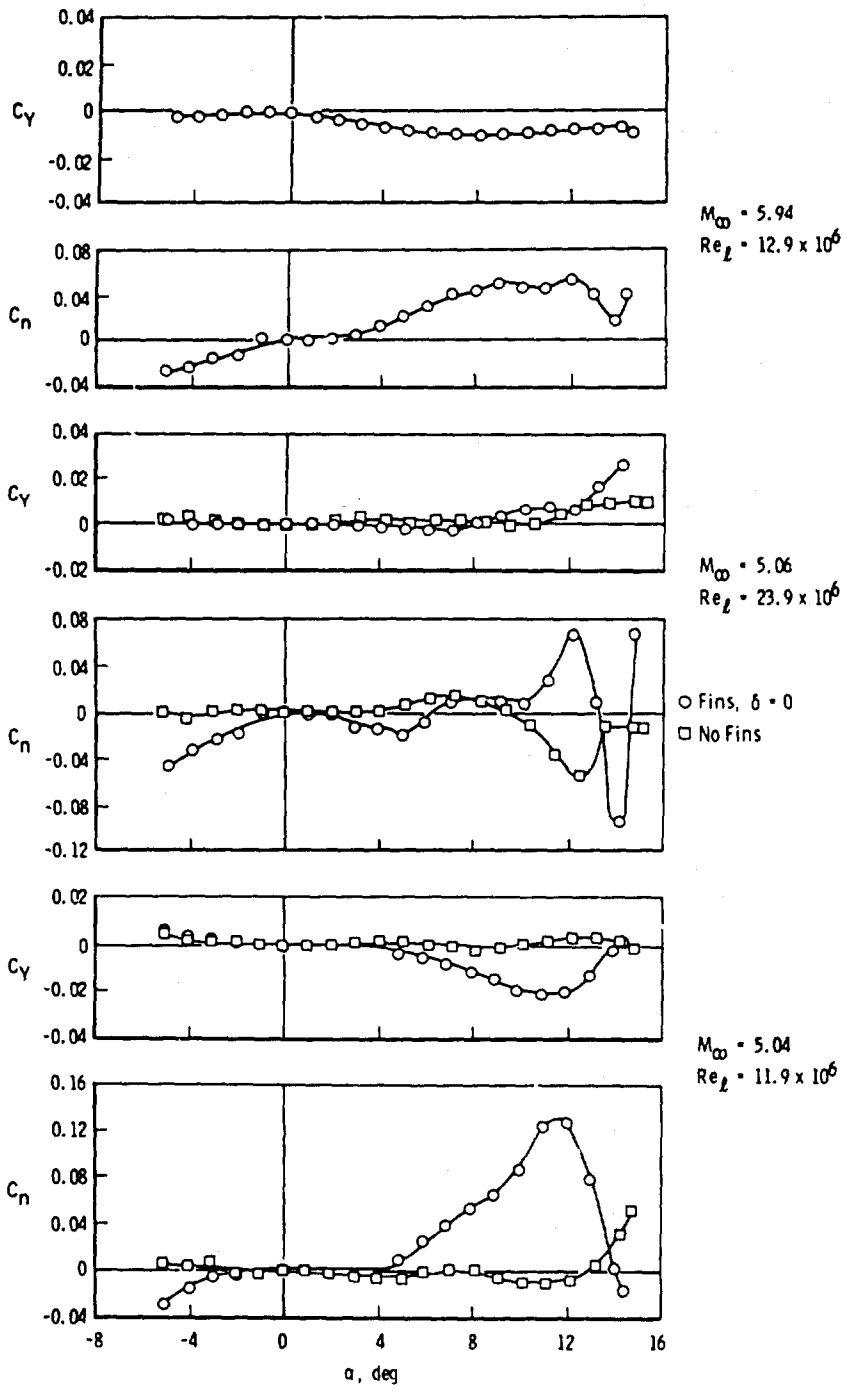

c. M_∞ = 5 and 6

Fig. 4 Concluded

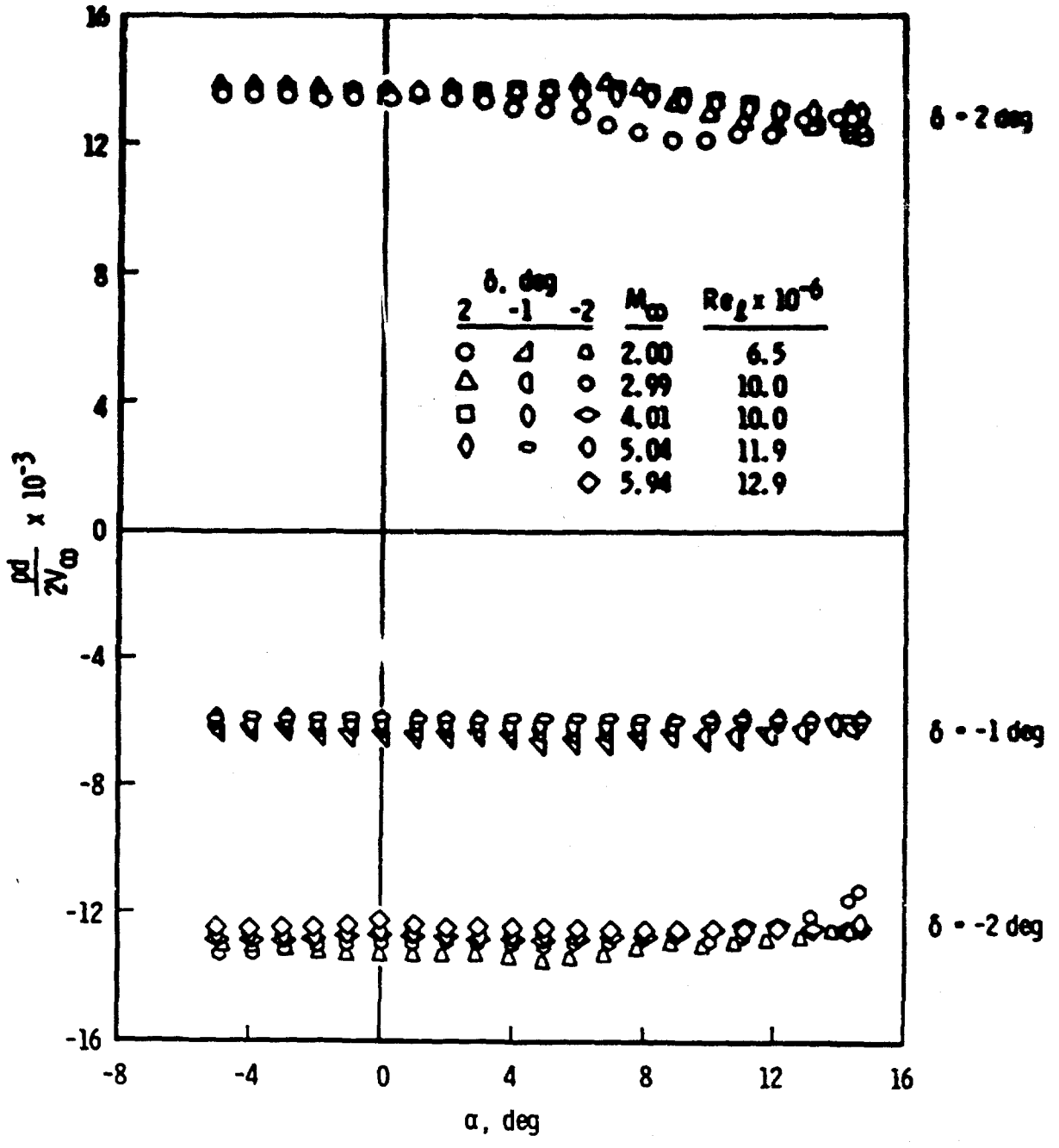

Fig. 6 Variation of Spin Parameter ($pd/2V_\infty$) with α

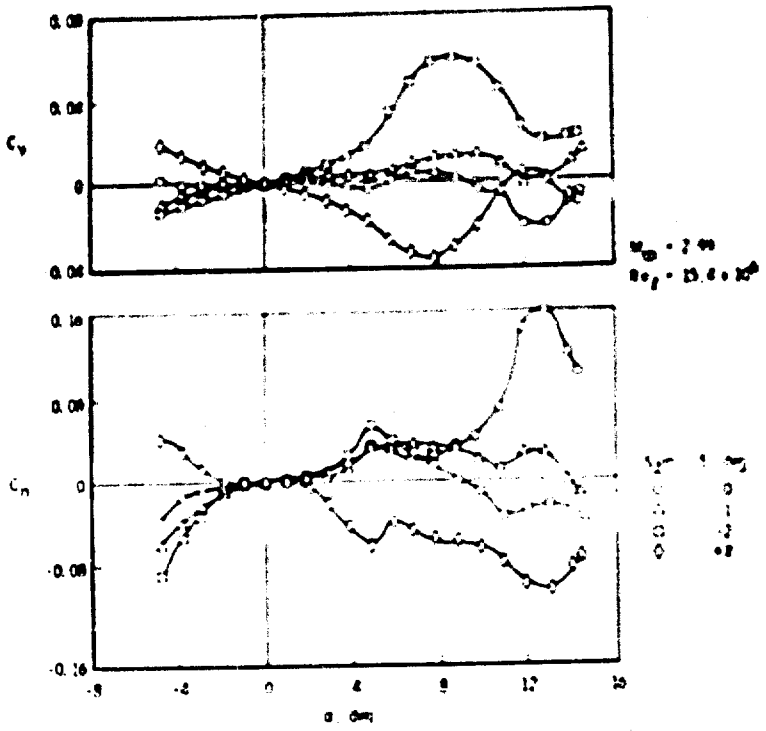

a. $M_\infty = 3$

Fig. 7 Variations of C_Y and C_n with α for δ = 0, -1, -2, and 2 deg

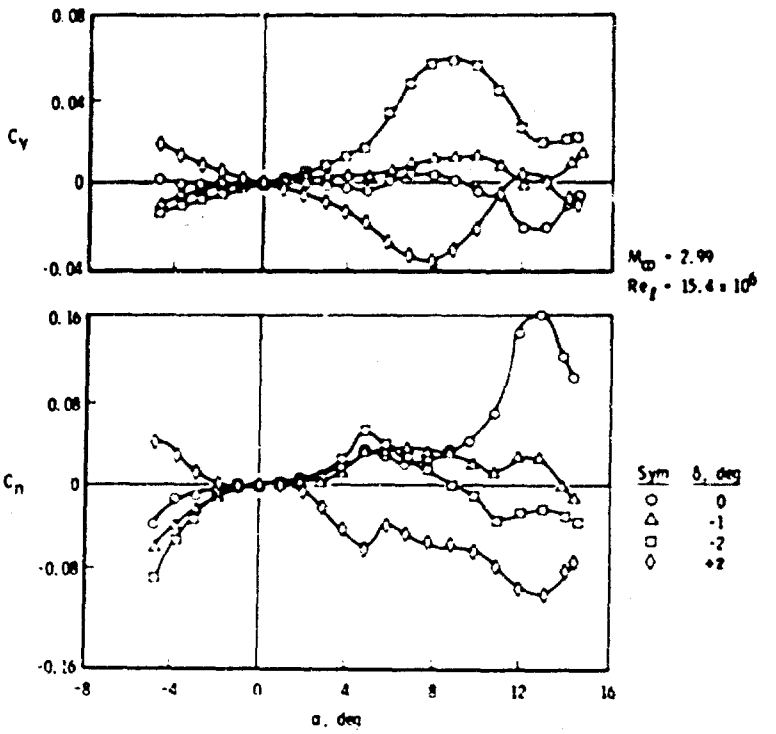

a. M_∞ = 3

Fig. 7 Variations of C_Y and C_n with α for δ = 0, -1, -2, and 2 deg

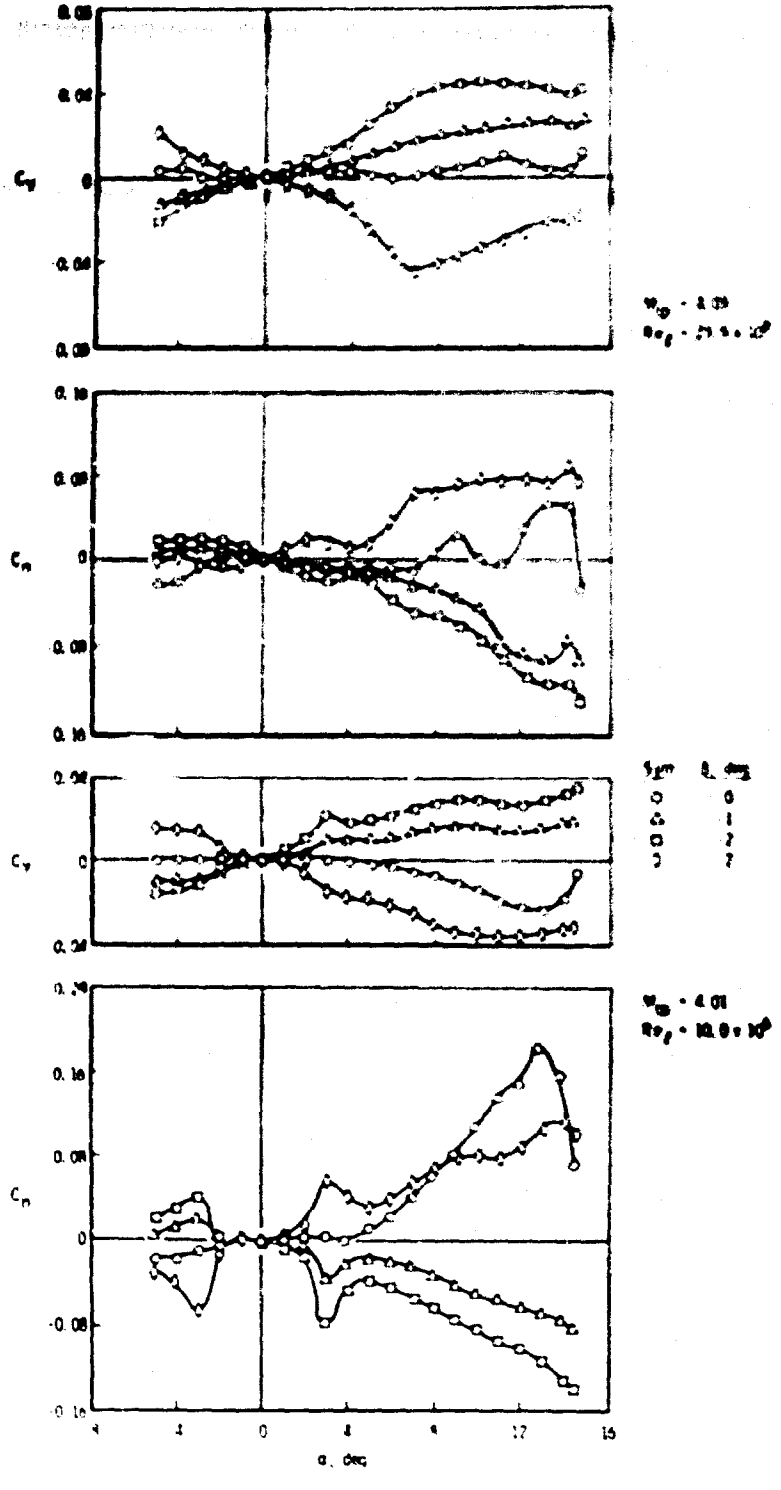

b. $M_\infty = 4$

Fig. 7 Continued

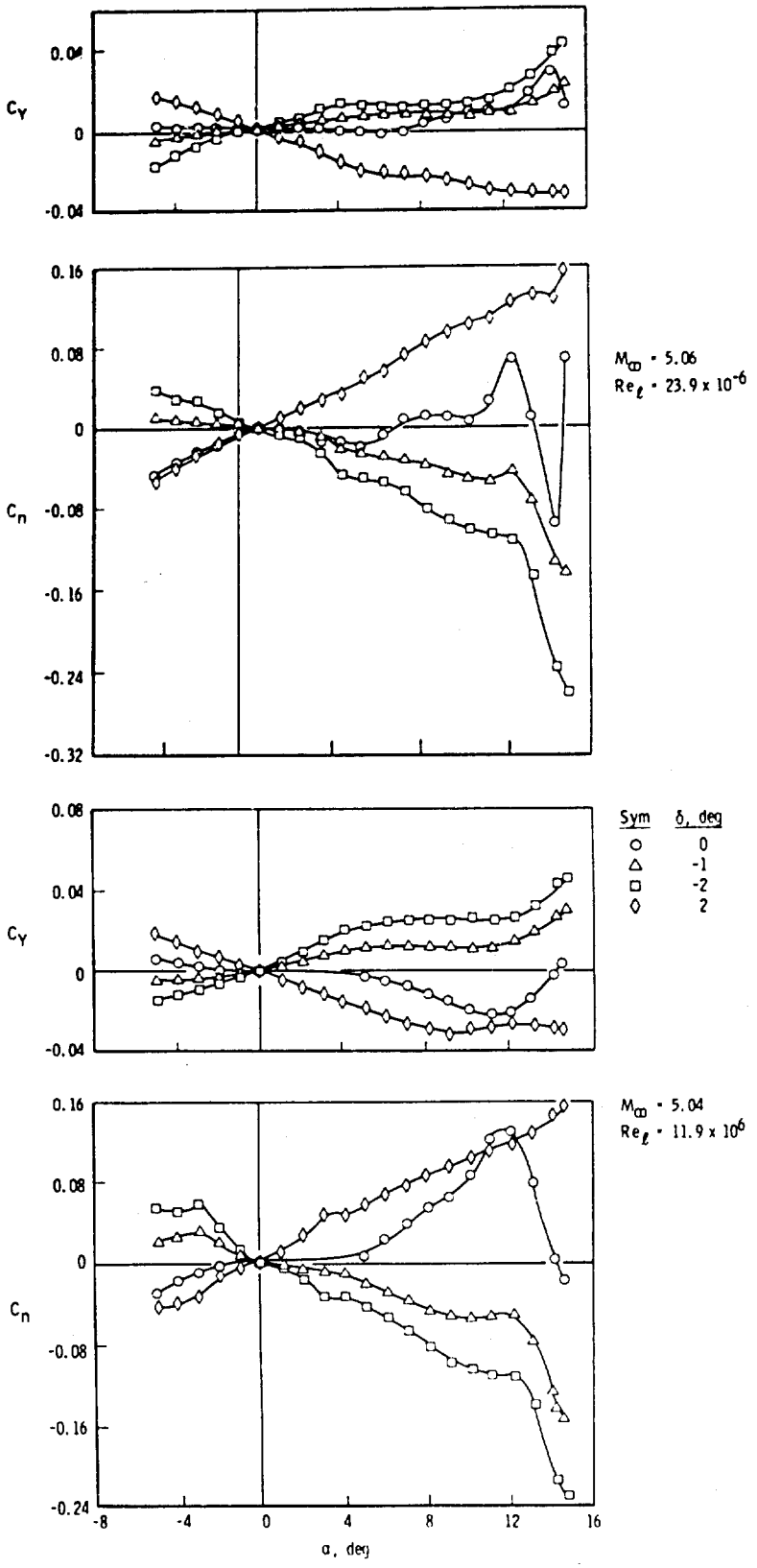

c. M_∞ = 5

Fig. 7 Concluded

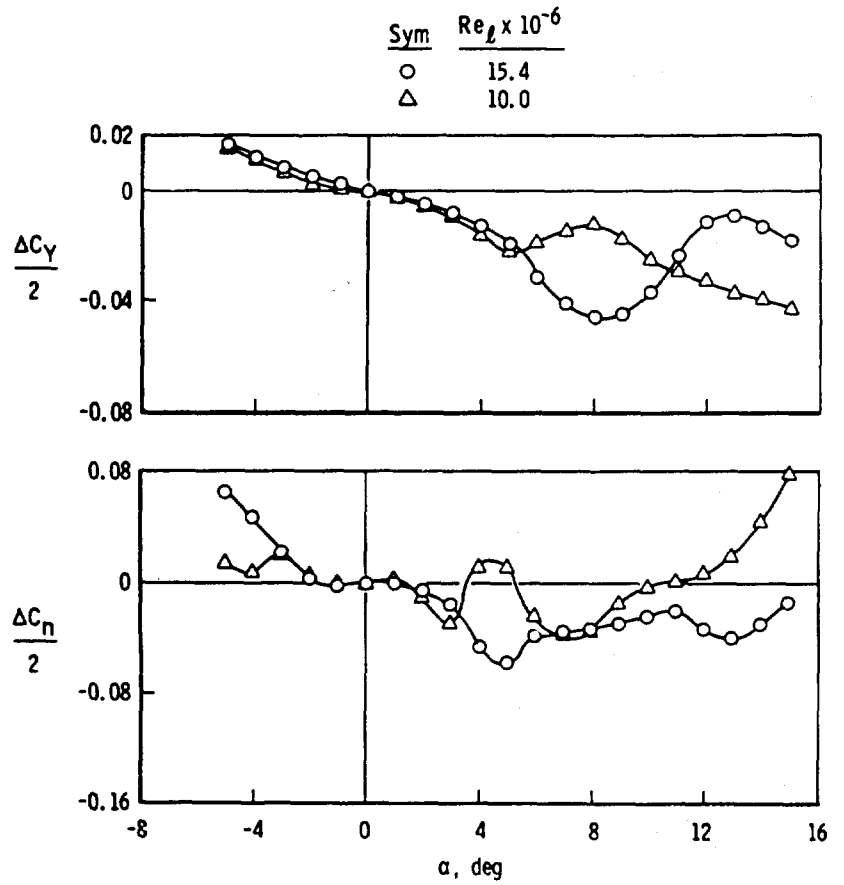

a. $M_\infty = 3$

Fig. 8 Variation of $\Delta C_Y/2$ and $\Delta C_n/2$ with α for $\delta = 2$ deg

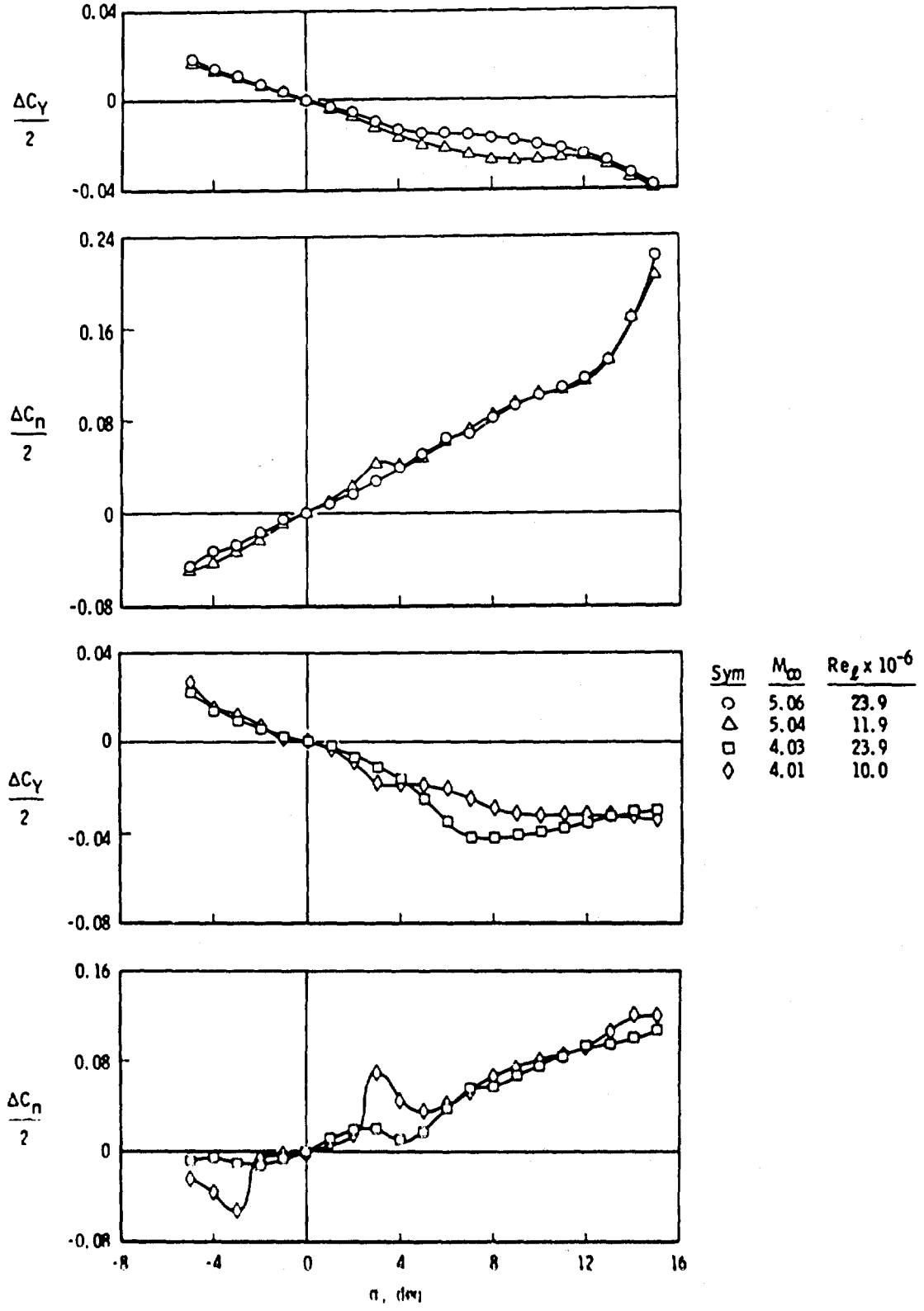

b. M_∞ 4 and 5

Fig. 8 Concluded

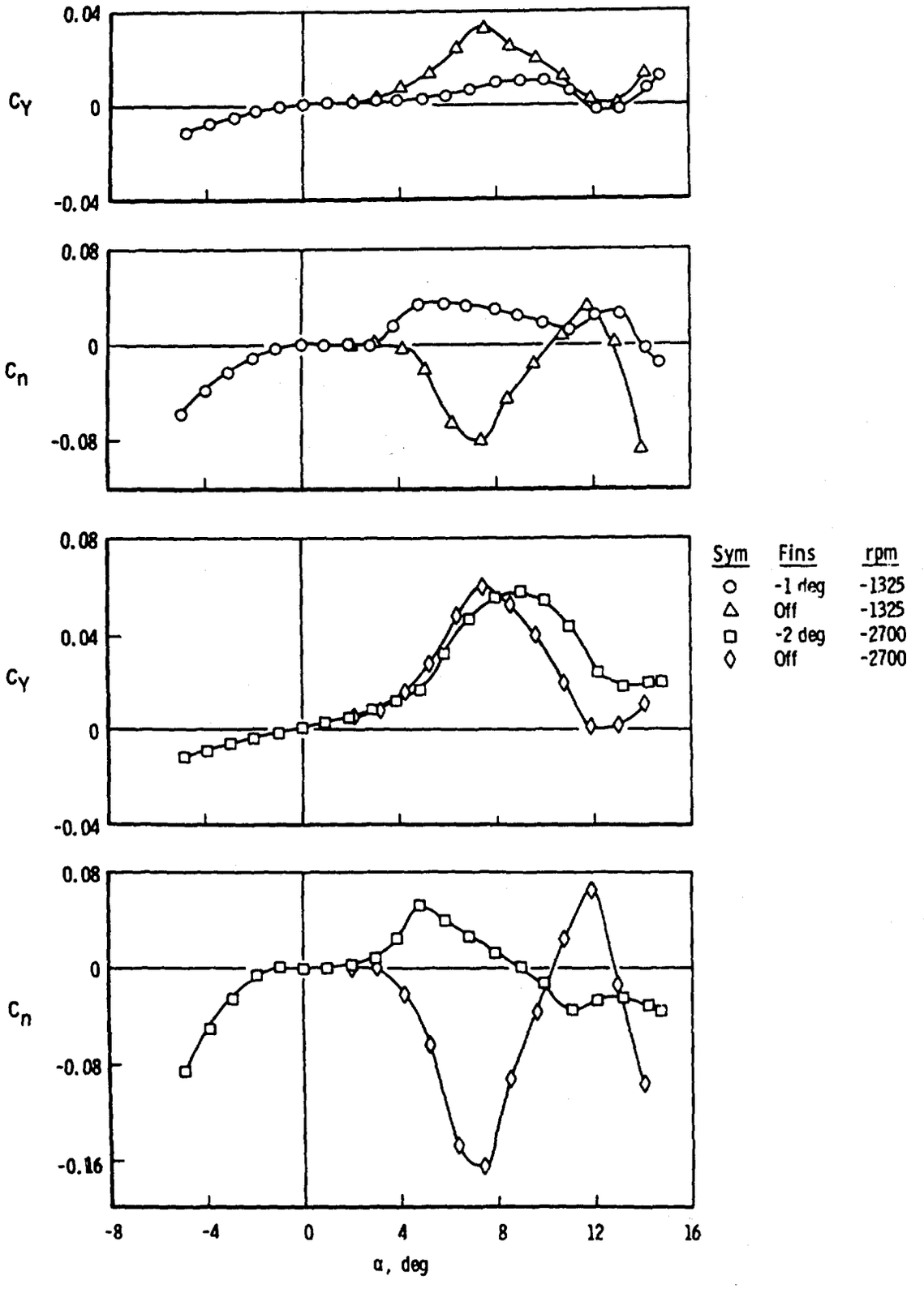

a. $M_\infty = 3$, $Re_\ell = 15.4 \times 10^6$

Fig. 9 Effects of Fins on the C_Y and C_n Variations with α

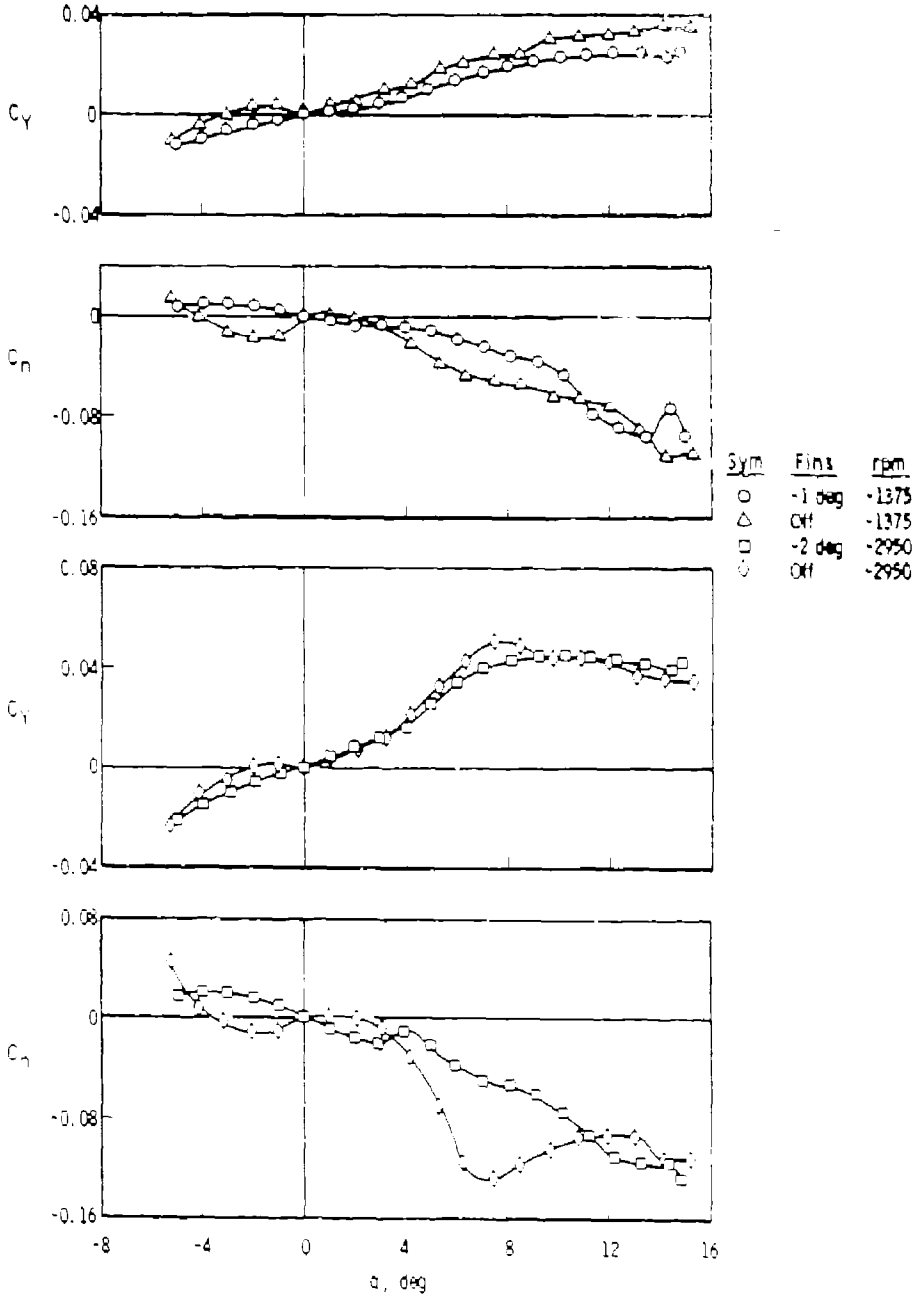

b. $M_\infty = 4$, $Re_f = 23.9 \cdot 10^6$

Fig. 9 Continued

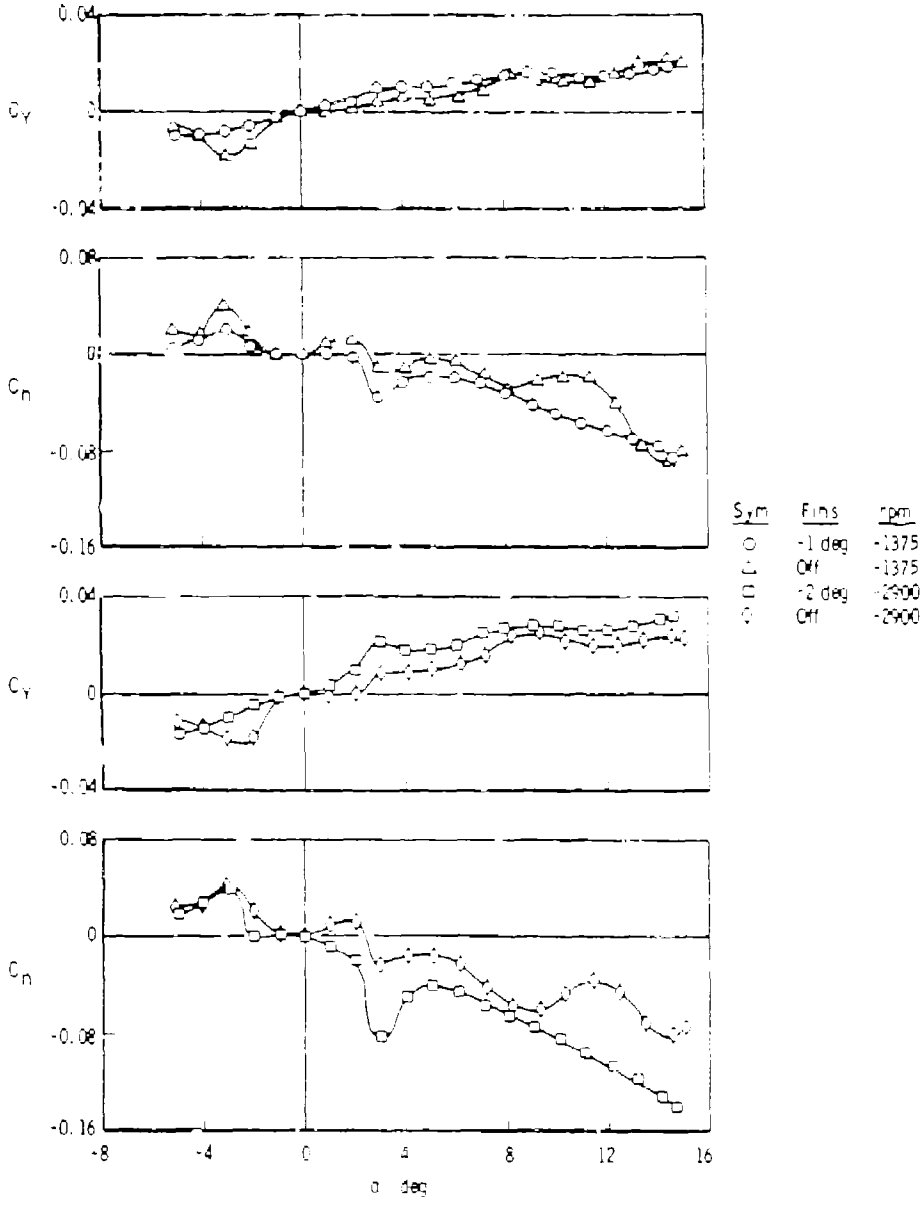

c. $M_\infty = 4$, $Re_j = 10.0 \times 10^6$

Fig. 9 Continued

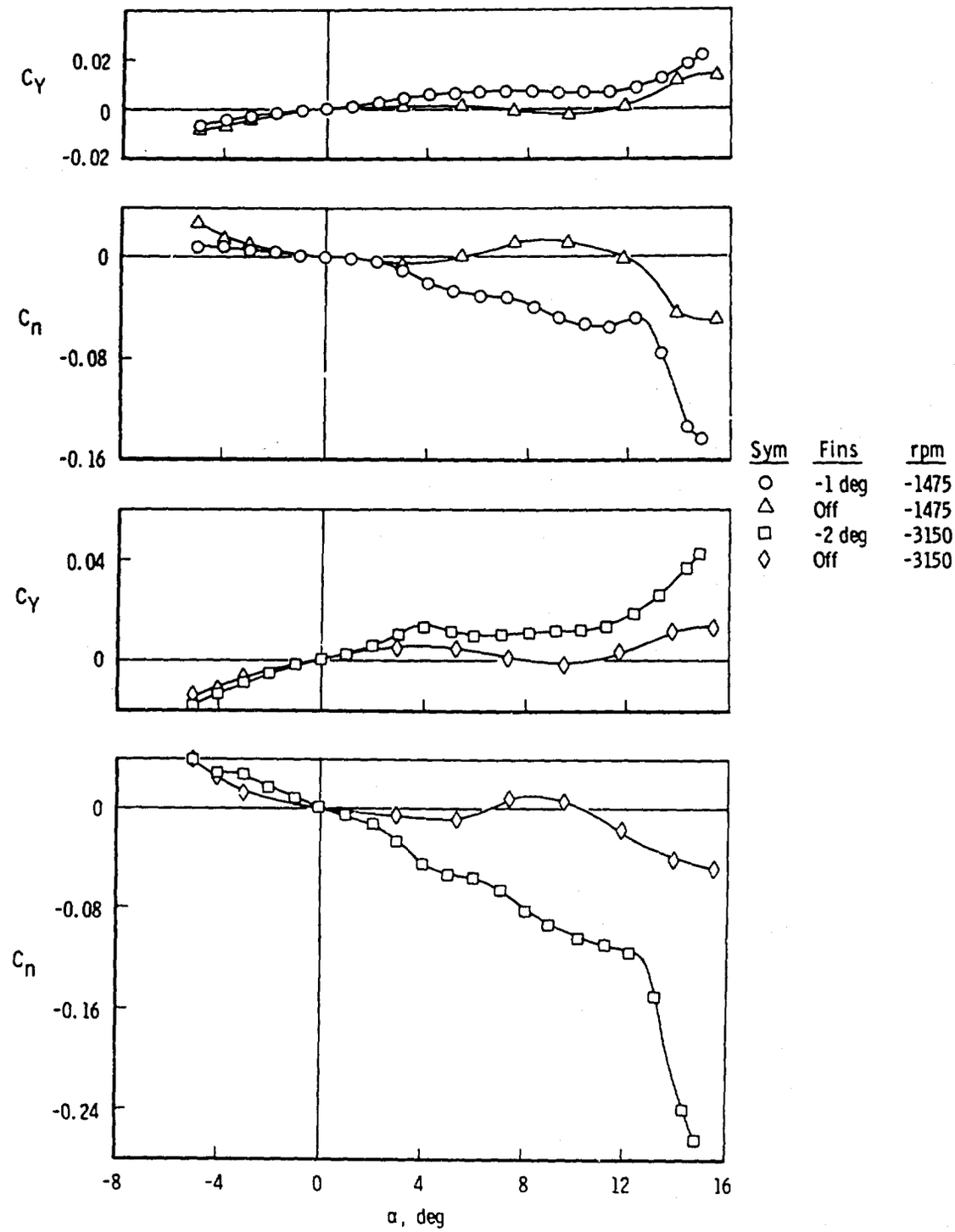

d. $M_\infty = 5$, $Re_\ell = 23.9 \times 10^6$

Fig. 9 Concluded

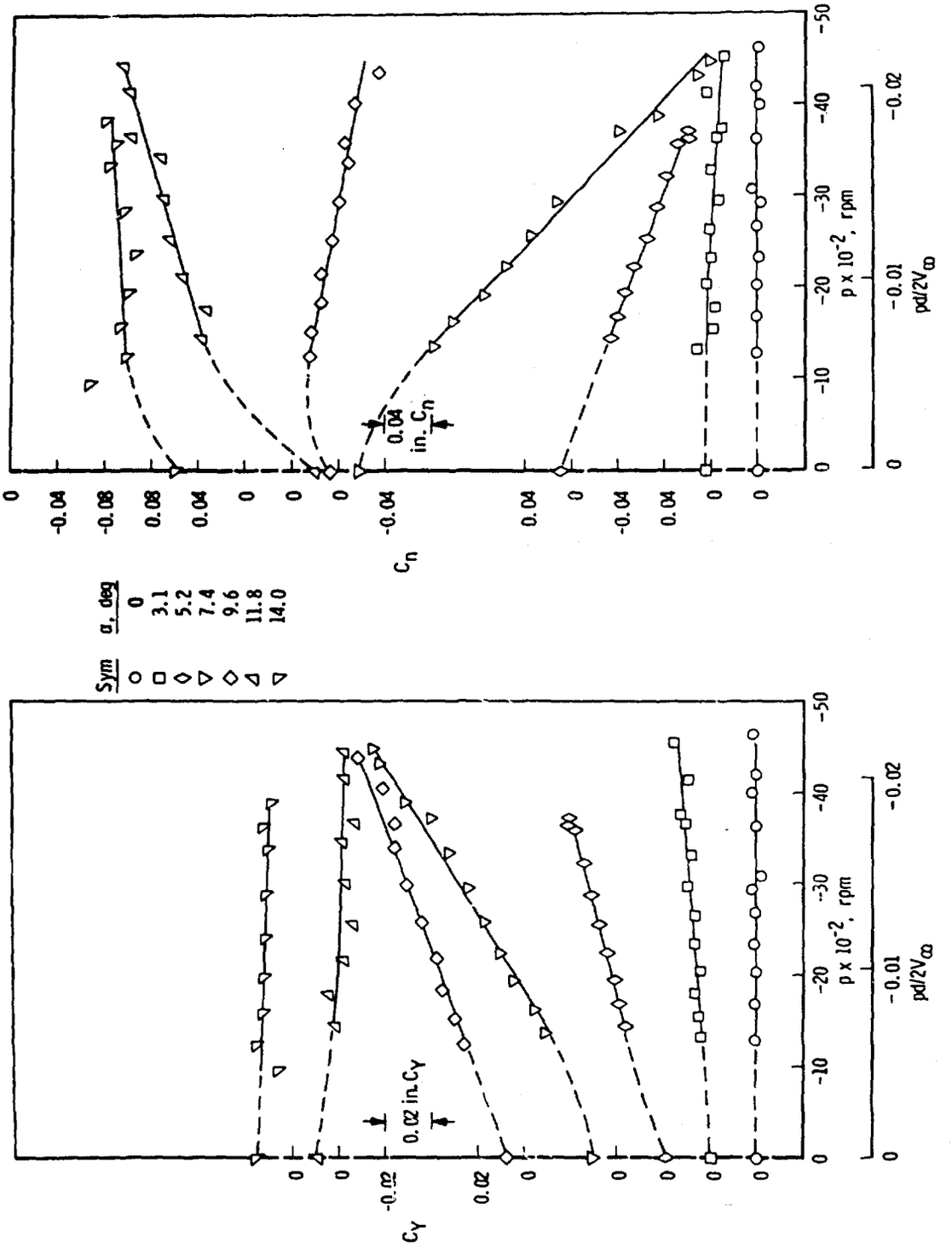

a. $M_\infty = 3$, $Re_\ell = 15.4 \times 10^6$

Fig. 10 Variation of C_Y and C_n with p for the Fins-Off Configuration

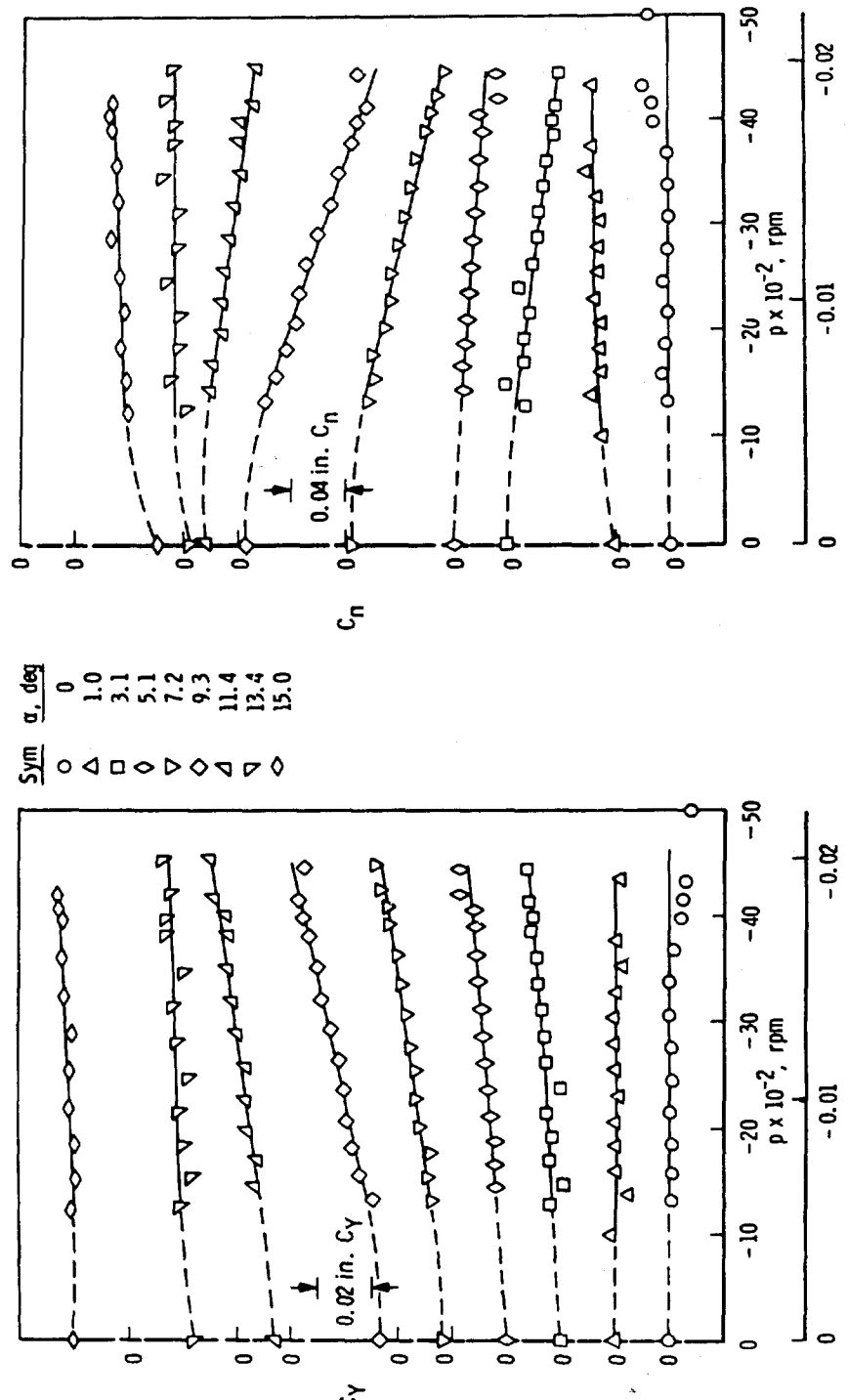

b. $M_\infty = 4$, $Re_\ell = 10.0 \times 10^6$

Fig. 10 Continued

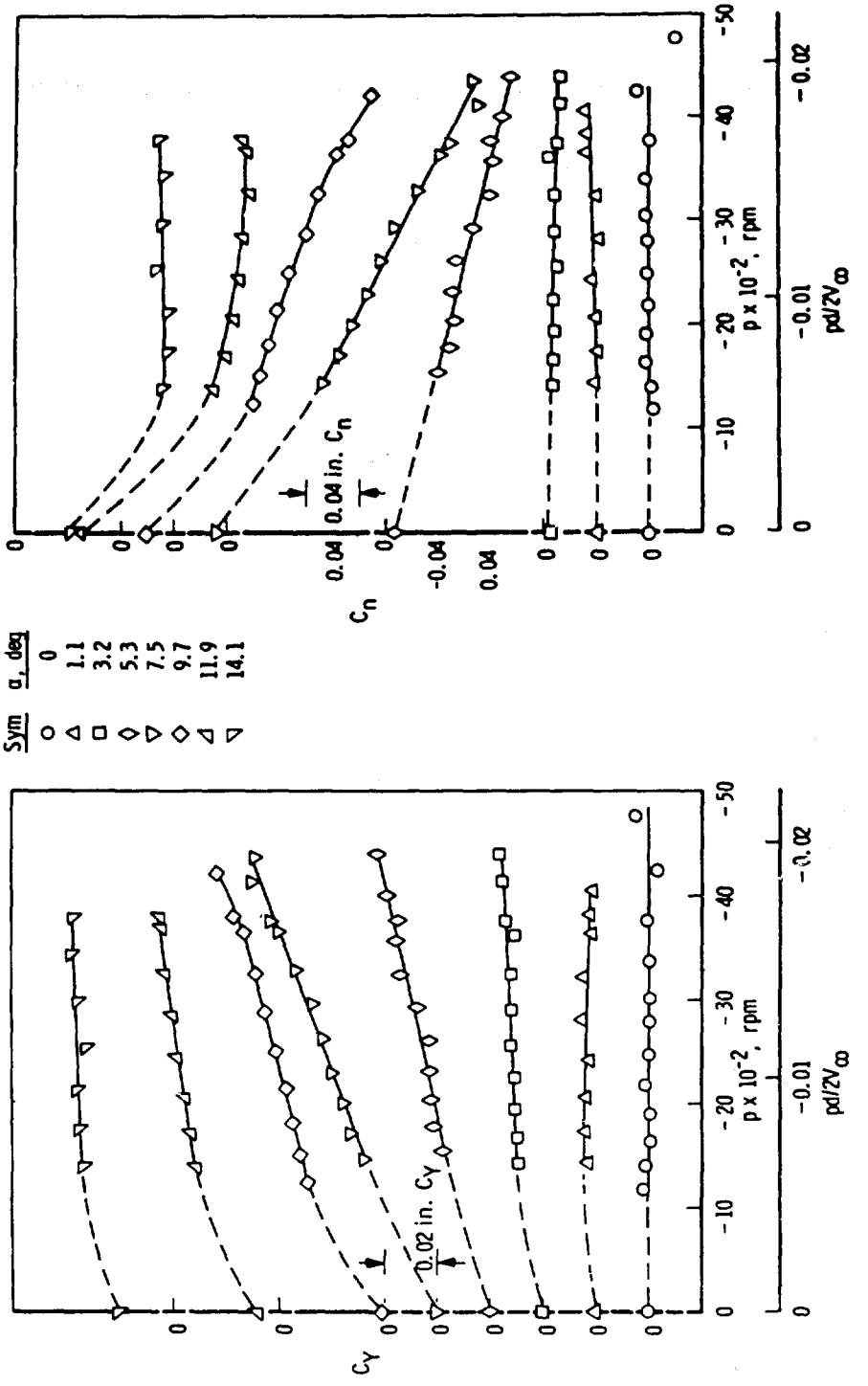

c. M_∞ = 4, Re_ℓ = 23.9 × 10^6

Fig. 10 Continued

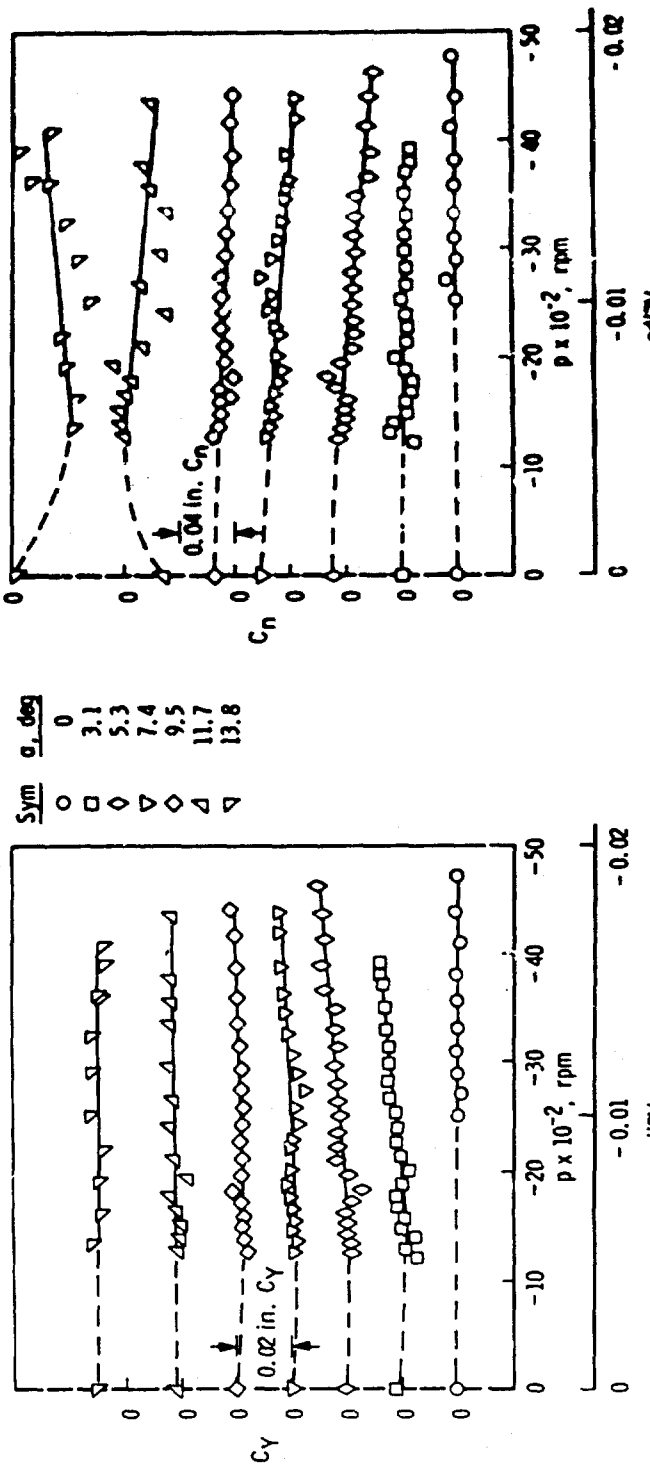

d. M_∞ = 5, Reℓ = 23.9 × 10^6

Fig. 10 Concluded

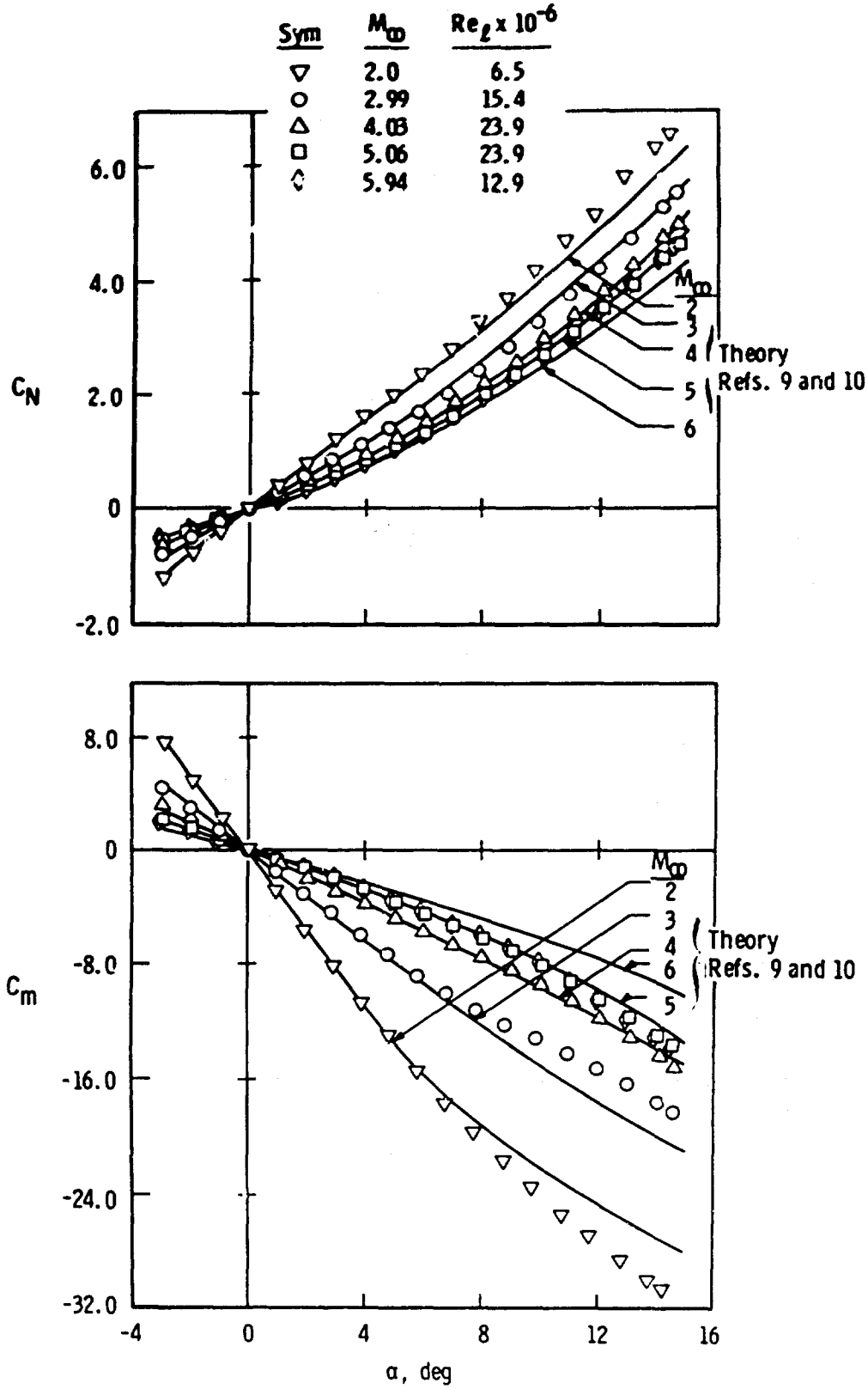

Fig. 11 C_N and C_m Variations with α for Fins-On (δ = 0)

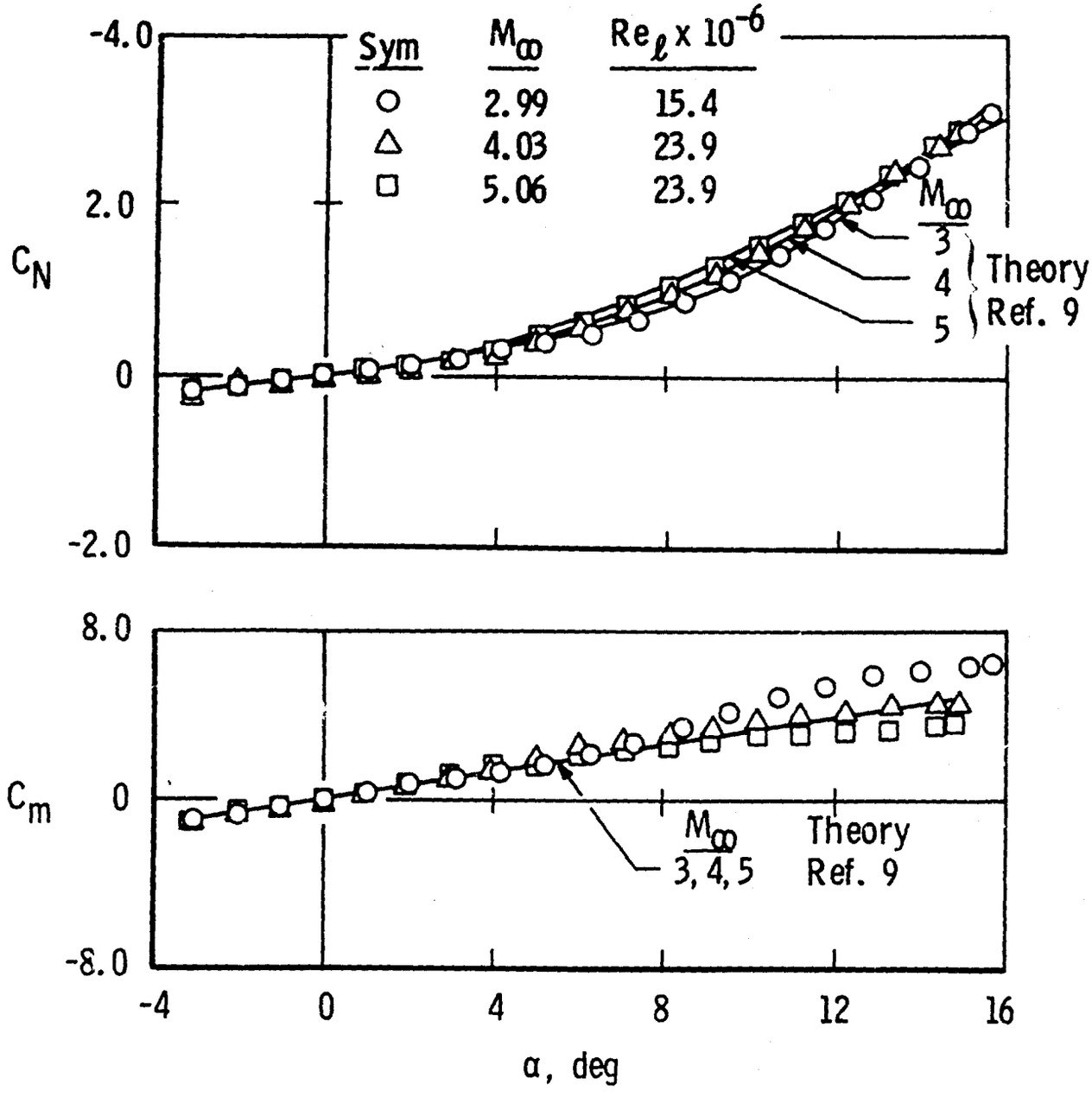

Fig. 12 C_N and C_m Variations with α for Fins-Off

TABLE I
TEST SUMMARY

M_∞	p_o, psia	T_o, °R	q_∞, psia	V_∞, ft/sec	$Re_\ell \times 10^{-6}$	Fins-On δ, deg				Fins-Off	
						0	2	-1	-2	No Spin	Spin
2.00	6.3	555	2.3	1706	6.5	x	x	x	x		
2.99	17.0	574	2.9	2102	10.0	x	x	x	x	x	x
2.99	26.0	575	4.5	2102	15.4	x	x	x	x	x	x
4.01	28.0	576	2.1	2287	10.0	x	x	x	x	x	x
4.03	70.0	575	5.0	2293	23.9	x	x	x	x	x	x
5.04	62.0	605	1.9	2485	11.9	x	x	x	x	x	
5.06	135.0	637	4.3	2530	23.9	x	x	x	x	x	x
5.94	107.0	642	1.8	2596	12.9	x					

x Data taken at angles of attack from -5 to 15 deg.
Note: For p and $pd/2V_\infty$ values, see Figs. 5, 6, and 10.

UNCLASSIFIED

Security Classification

DOCUMENT CONTROL DATA - R & D

(Security classification of title, body of abstract and indexing annotation must be entered when the overall report is classified)

1. ORIGINATING ACTIVITY (Corporate author)
Arnold Engineering Development Center
ARO, Inc., Operating Contractor
Arnold Air Force Station, Tennessee 37389

2a. REPORT SECURITY CLASSIFICATION
UNCLASSIFIED

2b. GROUP
N/A

3. REPORT TITLE

WIND TUNNEL TESTS ON THE APACHE SOUNDING ROCKET WITH VARIOUS SPIN RATES AT SUPERSONIC SPEEDS

4. DESCRIPTIVE NOTES (Type of report and inclusive dates)
December 9 to December 17, 1968 - Final Report

5. AUTHOR(S) (First name, middle initial, last name)

James C. Uselton and Jack B. Carman, ARO, Inc.

6. REPORT DATE	7a. TOTAL NO. OF PAGES	7b. NO. OF REFS
May 1969	41	10

8a. CONTRACT OR GRANT NO.	9a. ORIGINATOR'S REPORT NUMBER(S)
F40600-69-C-0001 b. PROJECT NO. 2547 c. Program Element 62701F	AEDC-TR-69-57
	9b. OTHER REPORT NO(S) (Any other numbers that may be assigned this report) N/A

10. DISTRIBUTION STATEMENT
This document has been approved for public release and sale; its distribution is unlimited.

11. SUPPLEMENTARY NOTES	12. SPONSORING MILITARY ACTIVITY
Available in DDC.	Air Force Armament Laboratory (ATBR) Eglin AF Base, Florida 32542

13. ABSTRACT

Aerodynamic characteristics were investigated for a 0.355-scale model of the Apache sounding rocket at Mach numbers 2 to 6. Free-stream Reynolds number, based on model length, was varied between 6.5×10^6 and 23.9×10^6, and angle of attack varied from -5 to 15 deg. The model was tested without fins at spin rates up to 4,000 rpm and with fins at cant angles of 0, -1, and ±2 deg, which produced spin rates ranging from about -3200 to 3200 rpm. Tests of the complete spinning model showed significant changes in side loading with angle of attack, Mach number, and Reynolds number. Tests of the model with and without fins allowed a degree of accessment of the relative body and fin Magnus contributions. Tests of the nonspinning model with and without fins showed significant side loads attributed to steady asymmetric leeward vortex patterns.

DD FORM 1 NOV 65 1473

UNCLASSIFIED

Security Classification

14. KEY WORDS	LINK A		LINK B		LINK C	
	ROLE	WT	ROLE	WT	ROLE	WT
supersonic wind tunnels						
aerodynamic characteristics						
rocket models						
fins						
Apache						
sounding rockets						
spin stabilization						
Magnus effect						